

The abundance of ^{36}S in IRC+10216 and its production in the Galaxy

R. Mauersberger¹, U. Ott², C. Henkel³, J. Cernicharo⁴, and R. Gallino^{5,6}

¹ Instituto de Radioastronomía Milimétrica, Avda. Divina Pastora 7, Local 20, E-18012 Granada, Spain

² Max-Planck-Institut für Chemie, Becherweg 27, D-55128 Mainz, Germany

³ Max-Planck-Institut für Radioastronomie, Auf dem Hügel 69, D-53121 Bonn, Germany

⁴ Instituto de la Estructura de la Materia, Dept. de Astronomía Molecular e Infrarroja, Serrano 113, E-28006 Madrid, Spain

⁵ Dipartimento di Fisica Generale dell'Università di Torino, Via Pietro Giuria 1, I-10125 Torino, Italy

⁶ Centre for Stellar and Planetary Sciences, Monash University, Melbourne 3800, Australia

Received ; accepted 21.6.2004

Abstract. The $J = 2 - 1$ and $3 - 2$ rotational lines of the rare isotopomer C^{36}S and the $J = 5 - 4$ and $6 - 5$ transitions of Si^{36}S were detected in the carbon star IRC+10216 (CW Leo). These are the first detections of ^{36}S bearing molecules in a star and the first spectroscopic detection of Si^{36}S . From a comparison of ^{34}S and ^{36}S bearing isotopomers, the $^{34}\text{S}/^{36}\text{S}$ isotopic ratio is $107(\pm 15)$. This value is comparable to values in the interstellar medium of the inner Galactic disk (115) but is smaller than the solar value of 288 (Ding et al. 2001). The increase of the ^{36}S abundance relative to ^{34}S only qualitatively follows model predictions of a low mass AGB star. Quantitative agreement of the observed $^{34}\text{S}/^{36}\text{S}$ ratio with the stellar models can be reached if the age of IRC+10216 and Galactic chemical evolution are taken into account. Other less likely possibilities are the presence of considerable inhomogeneities in the interstellar medium and either IRC+10216 or the Sun started with a peculiar ^{36}S abundance. Other production mechanisms potentially capable of enhancing the Galactic interstellar medium are discussed. From the observed line density toward IRC+10216 and toward Galactic star forming regions, we estimate the confusion limit toward those sources.

Key words. nuclear reactions, nucleosynthesis, abundances – stars: abundances – stars: AGB and post-AGB-stars: individual: IRC+10216 – ISM: abundances – radiolines: stars

1. Introduction

Heavy elements are formed in stars of medium or high mass. At the end of their lifetimes, these stars recycle, via winds or via explosions, a fraction of these metals back into the interstellar medium (ISM). Over the aeons, interstellar abundances of such heavy elements have been increasing and isotopic compositions have been changing, as can be seen by comparing the composition of the present day ISM with that of Damped Lyman- α systems (Rauch 1998). Not only elemental but also isotopic abundances, which are mainly determined in the radio range, are powerful tools to investigate stellar production sites and the star forming history of galaxies (Wilson & Matteucci 1992; Henkel & Mauersberger 1993; Henkel et al. 1994; Wilson & Rood 1994; Kahane 1995; Prantzos et al. 1996; Bieging 1997; Henkel et al. 1998).

Being one of the ten most abundant elements and possessing four stable isotopes, sulfur is of particular interest for such studies. Relative abundances of stable sulfur isotopes have been determined for meteorites (e.g. Gao & Thiemens 1991), the Moon (Thode & Rees 1971), the Galactic ISM (e.g. Chin et al. 1996), Cosmic Rays (Thayer 1997) and late type stars (e.g. Kahane et al. 1988). Even in external galaxies $^{32}\text{S}/^{34}\text{S}$ ratios could be measured (Mauersberger & Henkel 1989; Johansson et al. 1994). Small isotopic variations of sulfur in terrestrial, meteoric and planetary samples have been proposed to be powerful indicators of chemical, geophysical and biological processes (Canfield 2001; Farquhar & Wing 2003)

Mauersberger et al. (1996) presented the first interstellar detections of a ^{36}S bearing molecule toward a number of Galactic hot cores. While the solar $^{34}\text{S}/^{36}\text{S}$ ratio is 288, an interstellar ratio of $115(\pm 17)$ was found. This supported the notion that unlike other S isotopes, ^{36}S is a secondary-like nucleus, predominantly synthesized via the

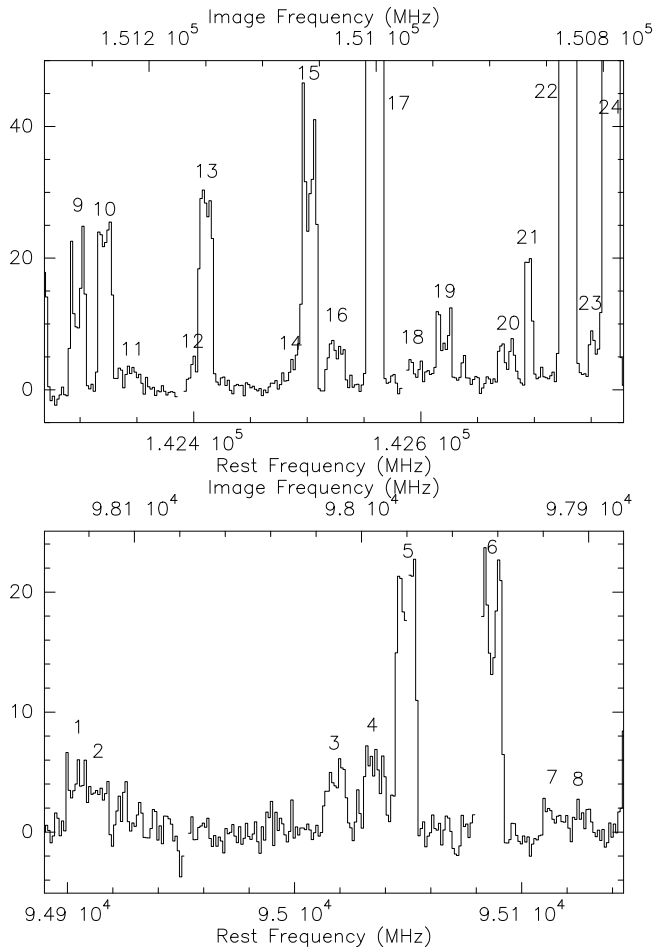


Fig. 1. The whole spectral range measured near the C^{36}S $J = 2 - 1$ (lower panel) and $3 - 2$ (upper panel) transitions toward IRC+10216. The channel spacing corresponds to 3.1 km s^{-1} for the 3 mm spectrum and 4.2 km s^{-1} for the 2 mm spectrum. The intensity is in mK (T_{A}^*). For identifications, see the Appendix A.

s-process in massive stars. Most interstellar $^{34}\text{S}/^{36}\text{S}$ ratios were determined, however, for sources with galactocentric distances $R_{\text{GC}} \leq 7 \text{ kpc}$. A positive $^{34}\text{S}/^{36}\text{S}$ gradient with increasing R_{GC} , i.e. a ratio between 115 and ~ 180 in the solar neighborhood, is not completely ruled out by the data of Mauersberger et al. (1996).

In order to further constrain the production site of ^{36}S in the Galaxy, we conducted a search for rotational lines of C^{36}S and Si^{36}S toward the prototypical carbon star IRC+10216, where all other stable S isotopes have been detected previously (Kahane et al. 1988).

2. Line frequencies

The rest frequencies of the C^{36}S $J = 2 - 1$ and $3 - 2$ lines are 95.0167 and 142.5228 GHz (V. Ahrens, pers. comm.), and 96.4130 and 144.6171 GHz for the corresponding C^{34}S lines (Lovas 1992).

The frequencies of Si^{36}S have not been measured in the laboratory. However, it is straightforward to derive the

rotational constants of Si^{36}S from those of SiS (see, e.g., Frum et al. 1990) using the isotopic relation for diatomic molecules (e.g. Townes & Schawlow 1975). For Si^{36}S , we derived $B_0 = 8607.47 \text{ MHz}$ and $D_0 = 5.4 \cdot 10^{-3} \text{ MHz}$. The computed frequencies are $\nu(J = 5 - 4) = 86071.984 \text{ MHz}$ and $\nu(J = 6 - 5) = 103284.96 \text{ MHz}$. The expected relative error for the rotational constants is $< 10^{-5}$ and the resulting expected uncertainty for the $J = 5 - 4$ and $6 - 5$ lines of Si^{36}S is $< 0.5 \text{ MHz}$. We have checked the precision of those relations for the different isotopes of SiS that have been measured in the laboratory and we find that the quoted uncertainties are rather conservative. Recently, Sanz et al. (2003) measured the rotational constants of several isotopes of SiS and have provided a fit, taking into account the breakdown of the Born-Oppenheimer approximation, to the data of all isotopes of SiS. From their constants we infer those of Si^{36}S to be $B_0 = 8607.495 \text{ MHz}$, $D_0 = 5.364 \cdot 10^{-3} \text{ MHz}$, $\nu(J = 5 - 4) = 86072.27 \text{ MHz}$ and $\nu(J = 6 - 5) = 103285.31 \text{ MHz}$, i.e. 0.3 MHz of difference with respect to our early calculations. Hence, we are confident that the calculated frequencies have an error well below 1 MHz.

3. Observations

The $J = 2 - 1$ and $J = 3 - 2$ lines of C^{34}S and C^{36}S were observed between October 1999 and September 2003 with the IRAM 30 m radiotelescope on Pico Veleta (Southern Spain) toward IRC+10216. The Si^{36}S observations were carried out between 1996 and 2003 at the same telescope. Several spectra at different frequency settings were observed for each line of Si^{36}S to ensure that the observed lines are coming from the signal side band. The observations were conducted under good weather conditions. SIS receivers were used with image sideband rejections of 20–25 dB. An antenna temperature (T_{A}^*) scale was established by a chopper wheel method. The forward efficiency of the telescope was 0.94 and the beam efficiencies were 0.80 at 3 mm and 0.65 at 2 mm. The beamwidth (full width at half maximum) of the 30 m antenna was $26''$ and $17''$ for the $2 - 1$ and $3 - 2$ transitions of the isotopomers of CS; for the $5 - 4$ and $6 - 5$ transitions of SiS, beamwidths were $28''$ and $24''$. From scans of continuum sources, we estimate the pointing to be correct within $5''$.

As backends, we employed filterbanks with 256 channels and a channel spacing of 1 MHz corresponding to $\sim 3.1 \text{ km s}^{-1}$ for the 3 mm transitions and 2.1 km s^{-1} for the 2 mm transitions. Two receivers were employed simultaneously, either observing orthogonal polarizations at the same wavelength or measuring one line at 2 mm and the other at 3 mm using just one polarization for each wavelength.

All spectral lines were measured using the wobbling secondary mirror with a beam throw of $200''$ in azimuth. The phase time was 2 seconds and the on-source integration of each subscan was 30 seconds. Subscans obtained by wobbling to the left and to the right of our source were

Table 1. Line parameters

Transition	$\int T_{\text{A}}^* dv$ mK km s $^{-1}$	v_{LSR} km s $^{-1}$	v_{exp} km s $^{-1}$	$\frac{C}{H}$ ^a
CS $J = 2 - 1$				
C ^{34}S	11600(100)	-26.2	14.0	0.55
C ^{36}S	96(21)	-26.2 ^b	14.0 ^b	0.55 ^b
C $^{36}\text{S}/\text{C}^{34}\text{S}$	8.3(1.8) 10^{-3} ^d			
CS $J = 3 - 2$				
C ^{34}S	22190(93)	-26.0	14.5	0.64
C ^{36}S	170(81)	-26.0 ^b	14.5 ^b	0.64 ^b
C $^{36}\text{S}/\text{C}^{34}\text{S}$	7.7(3.7) 10^{-3} ^d			
SiS $J = 5 - 4$				
Si ^{34}S	3180(80)	-26.4	14.4	0.82
Si ^{36}S	41(9)	-26.4 ^b	14.4 ^b	0.82 ^b
Si $^{36}\text{S}/\text{Si}^{34}\text{S}$	12.9(2.8) 10^{-3} ^d			
SiS $J = 6 - 5$				
Si ^{34}S	4280(70)	-26.5	14.1	0.76
Si ^{36}S ^c	40(18)	-26.5 ^b	14.1 ^b	0.76 ^b
Si $^{36}\text{S}/\text{Si}^{34}\text{S}$	9.3(4.2) 10^{-3} ^d			

a) the ratio between the intensities at the central velocity of the line and at the velocity of the horns (i.e. maximum blue or red shifted emission); b) fixed to values obtained for the C ^{34}S or Si ^{34}S lines; c) simultaneous fit with a blended, unidentified line at $\nu = 103.2804$ GHz and an intensity of 46(18) K km s $^{-1}$; d) from the integrated intensities yielded by the fits to the lines of ^{34}S and ^{36}S bearing species. The error given is the 1σ error from the fit and does not contain an estimate of systematic errors, e.g. due to baseline uncertainties.

added to eliminate baseline ripples caused by the asymmetry in the beam path (symmetric switching).

4. Results

Fig. 1 displays the entire spectral range measured at the frequencies of the C ^{36}S lines. Figs. 2 and 3 show the C ^{34}S , C ^{36}S , Si ^{34}S and Si ^{36}S spectra that are discussed in Sect. 5.2 in more detail. An inspection of Fig. 1 shows that a main source of uncertainty in the identification of weak lines and also in the definition of spectral baselines comes from the presence of many weak line features, in particular at 2 mm. In Appendix A, we list the line parameters of all features together with possible identifications. The Si ^{36}S data, showing a statistical behavior that is similar to the C ^{36}S data, will be analyzed elsewhere (Cernicharo et al., in prep.).

From the spectra, we subtracted baselines of first order. For the 3–2 line of C ^{36}S , almost the entire frequency range is covered with line features near or above the detection threshold making the identification of a region free of emission a difficult task. We chose spectral regions with particularly low emission for the definition of a baseline.

5. Discussion

5.1. Where is the confusion limit toward IRC+10216?

As it can be seen in Fig. 1 showing the total spectral range of 2×256 MHz toward IRC+10216, we have de-

tected a large number of spectral line features, many of them unidentified. There are more lines at 2 mm than at 3 mm although the rms of the data is similar. The spectral line density in our 2 mm spectrum is 15 lines per 256 MHz. Since each line has a width of about 14.5 MHz, about 85% of the spectral range observed would be covered with detectable line emission if there were no overlap. The weakest feature we identified in Table A.1 at $\lambda=2$ mm has $T_{\text{A}}^*=3.5$ mK, although the rms noise of our 2 mm spectrum is about 0.5 mK for 4 km s $^{-1}$ wide velocity channels. Apparently lines weaker than about 3.5 mK have escaped detection not because of lacking signal-to-noise but because their number is so high that they are all blended and therefore cannot be easily distinguished.

At $\lambda = 3$ mm, 6 lines have been detected from the signal band in a 256 MHz wide range. Since each line has a width of 9 MHz, 21% of the spectral range observed is covered by detected lines. The weakest of those have a T_{A}^* of about 1.5 mK, which corresponds to the 3σ noise level at a velocity resolution of 10 km s $^{-1}$. In contrast to the situation at 2 mm, we have not yet reached the 3 mm confusion limit. Nevertheless, at 3 mm we also see signs of weak blended lines at a level of ~ 1 mK. Weaker lines, on the order of 0.5 mK, have been identified recently (Cernicharo et al. 2004) making use of the characteristic line shapes of IRC+10216.

To summarize, at the IRAM 30-m telescope the confusion limit toward IRC+10216 is reached at $\lambda=2$ mm after integrating down to a system noise of about 1 mK, while at 3 mm one has to integrate down to 0.3 mK. For other well known molecular sources, confusion limits are given in Appendix B.

5.2. The identification of C ^{36}S and Si ^{36}S

As already mentioned in Sect. 4 there are emission features at the rest frequencies of both the 3–2 and the 2–1 lines of C ^{36}S . These clearly peak above the limits of line confusion. It turns out, however, that at 3 mm there are two emission lines of linear C $_3\text{H}$ from the image sideband, one of which coincides with the location of the expected C ^{36}S 2–1 feature. Also in the band is the image of the strong CS 2–1 line. From a well calibrated spectrum of these three lines (Mauersberger et al. 1989) we obtained their relative intensities. According to Cernicharo et al. (2000) there is no hint for variability in time, except for some very highly excited lines or maser lines. In our spectrum of C ^{36}S 2–1 (Fig. 2) we could therefore apply a fit to the CS line and the two C $_3\text{H}$ lines from the image band fixing the line shape and the relative intensities. When removing this composite fit from the spectrum, the residual still shows emission at the expected frequency of C ^{36}S (Fig. 2). This residual spectrum was used to determine the isotopic ratios given below.

We cannot exclude that the residual line is contaminated since a fit with fixed line shape and rest frequency to the line feature (to the values obtained for C ^{34}S) shows

some excess emission toward lower velocities. A possible contaminant of the $2 - 1$ line of C^{36}S is a series of K lines of the $J = 23 - 22$ transition of CH_3CCCN (methyl cyanoacetylene; Lovas 1984), which were detected toward a number of Galactic hot cores (Mauersberger et al. 1996). This is, however, unlikely, since this molecule is not yet identified toward IRC+10216 (e.g. Cernicharo et al. 2000).

We have used the procedure from the CLASS data reduction package to fit shell type circumstellar lines. In order to obtain more reliable values for the integrated intensities, we fixed some of the line parameters of ^{36}S bearing species to the values obtained from the more intense ^{34}S bearing isotopomers. Fit results are given in Table 1. In the fit to the C^{36}S $3 - 2$ line feature there is a hint for excess emission toward lower velocities. At that frequency, the only previously observed interstellar line in the Lovas (1984) catalog is a transition of CH_2CHCN (vinyl cyanide, $\nu = 142.523$ GHz). This complex molecule has never been detected before in IRC+10216 and the line strength is very low. It seems plausible that if there is contamination it comes from a transition of a molecule abundant in late type carbon stars but not in the ISM, such as C_7H and/or H_2C_6 (Guélin et al. 1997).

The Si^{36}S $5 - 4$ line can be well fitted, with the determination of the baseline being the major source of uncertainty. The Si^{36}S $6 - 5$ line is also clearly detected, although it seems to be blended with a weak, unidentified feature (Fig. 3). The parameters of the C^{34}S , C^{36}S , Si^{34}S , and Si^{36}S , lines and the derived $\text{C}^{34}\text{S}/\text{C}^{36}\text{S}$ and $\text{Si}^{34}\text{S}/\text{Si}^{36}\text{S}$ intensity ratios are given in Table 1. We can summarize that we have clearly detected C^{36}S and Si^{36}S in IRC+10216. These are the first detections of ^{36}S bearing molecules in a stellar atmosphere and the first detection of Si^{36}S outside the solar system.

5.3. The $^{34}\text{S}/^{36}\text{S}$ abundance ratio

The characteristic line profiles of spherically expanding molecular shells can be explained in terms of line opacity, expansion velocity and the relative sizes of the telescope beam and the stellar envelope (e.g. Kuiper et al. 1976; Olofsson et al. 1982). The slightly U-shaped profiles seen in C^{34}S and Si^{34}S can be explained by optically thin and spatially resolved emission. Optically thin lines are expected because the main isotopic lines are only moderately optically thick and because ^{34}S is a factor ~ 20 less abundant than the main isotope (Kahane et al. 1988; Cernicharo et al. 2000). Interferometric observations (Guélin et al. 1993; Lucas et al. 1995, for maps see Grewing 1994) confirm a compact condensation of about $10''$ diameter for main isotopic CS. SiS is even more compact (Lucas et al. 1995), which is also apparent by a comparison of C^{34}S and Si^{34}S line shapes (Figs. 2 and 3). It is safe to assume that also C^{36}S and Si^{36}S emission is optically thin and it is plausible that the distributions of ^{34}S and ^{36}S bearing isotopomers are similar. Chemical fractionation, as discussed in Chin et al. (1996), should be

negligible in the warm (50 K, Cernicharo et al. 2000) environment of the inner shell of IRC+10216. Since the isotopomers have very similar transition frequencies we can assume that the intensity ratios of corresponding transitions reflect the abundance ratios (for a discussion, see Kahane et al. 1988).

From Table 1 it is evident that the relative errors of the integrated line intensities of the ^{36}S bearing molecules are of the order of 20% or more, while the relative errors for the ^{34}S bearing species are much smaller. While it is relatively straightforward to determine the $\text{X}^{36}\text{S}/\text{X}^{34}\text{S}$ ratios from fitted line profiles (as summarized in Table 1), it is much more difficult to estimate the $\text{X}^{34}\text{S}/\text{X}^{36}\text{S}$ ratios since the simple rules for error propagation apply only if the relative errors are small. In addition, if we assume that the error distribution of the $\text{X}^{36}\text{S}/\text{X}^{34}\text{S}$ ratios is Gaussian, the distribution of the inverse ratio is not such a simple and symmetric function, making the determination of the variance difficult (see Chapter 3.3.3 in Wall & Jenkins 2003).

The errors as quoted have been calculated from the formal errors of the fits to the line profiles. From these four ratios, and using as weights the inverse squares of the formal errors of the individual ratios, we have determined the weighted mean of the $^{36}\text{S}/^{34}\text{S}$ abundance ratio and its error to be $0.0094(\pm 0.0013)$ (see e.g. Bevington & Robinson 1992). From a graphical representation of the individual values and their mean (see Fig. 5) the only transition whose abundance ratio deviates from the mean value is the SiS $5 - 4$ line. This might be an additional hint that for this line there is, in addition to the statistic uncertainty, also a systematic effect, for example a blend with an unidentified line (see the discussion above). Since the relative error of the average $^{36}\text{S}/^{34}\text{S}$ abundance ratio is only 14%, the expectation value of the $^{34}\text{S}/^{36}\text{S}$ ratio and its error can be easily determined. In the following we will use a $^{34}\text{S}/^{36}\text{S}$ ratio of $107(\pm 15)$ for IRC+10216 to ease a comparison with values published in the literature.

This value of the best fit is very similar to the interstellar value of $115(\pm 17)$ (Mauersberger et al. 1996) but is smaller than the solar system value of 288 (Ding et al. 2001). In Table 2, we give a compilation of all available estimates for sulfur isotope ratios.

5.4. The origin of ^{36}S

5.4.1. Solar abundance and nucleosynthesis of ^{36}S

^{36}S is one of the more enigmatic stable nuclei in nature. Partly because of its rarity (solar system isotopic abundance 0.015% relative to ^{32}S), and partly because it is rarely employed in mass spectrometric studies of sulfur isotopes, up to very recently even its solar system abundance was quite uncertain. The often used Anders & Grevesse (1989) abundance table lists the S isotopes with a $^{34}\text{S}/^{36}\text{S}$ ratio of 211 (no errors given). An updated value is recommended in the 1998 compilation of isotopic abundances of the International Union of Pure

Table 2. Isotopic ratios of sulfur^a

Ratio	solar system	ISM	C.R.	IRC+10216
$^{32}\text{S}/^{34}\text{S}$	22.64(0.00)	24.4(5) ^b	16(-5,+11)	21.8(2.6)
$^{32}\text{S}/^{33}\text{S}$	126.95(0.05)	~150	38(-18,+500)	121(15)
$^{32}\text{S}/^{36}\text{S}$	6519(20)	3280(760)		2700(600)
$^{34}\text{S}/^{33}\text{S}$	5.606(0.002)	6.3(1)		5.6(.3)
$^{34}\text{S}/^{36}\text{S}$	288(1)	115(17)		107(15)

a) References: solar system data: Canyon Diablo troilite (CDT), Ding et al. 2001; ISM data: Chin et al. (1996), Mauersberger et al. (1996), most ISM data are from the inner Galaxy; Cosmic Rays: these are “source abundances”, Thayer (1997); IRC+10216: Kahane et al. (2000), this paper.

b) the average value for sources at various galactocentric radii; the data by Chin et al. (1996) indicate a possible galactocentric $^{32}\text{S}/^{34}\text{S}$ abundance gradient, which would correspond to a value of $32(\pm 5)$ at the solar circle.

and Applied Chemistry, (Rosman & Taylor 1998), where a ratio $^{34}\text{S}/^{36}\text{S} = 248 \pm 29$ is listed as the “best measurement from a single terrestrial source”; this composition has also been used by Lodders (2003) for her Solar System abundance table. Sulfur isotope ratios measured in the laboratory are commonly reported as permill deviations from the Canyon Diablo Troilite (V-CDT) standard, which has an S isotopic composition fairly representative for Solar system materials (IUPAC 2003 compilation; de Laeter et al., 2003). Its composition has recently been precisely redetermined, with a $^{34}\text{S}/^{36}\text{S}$ ratio of 288 ± 1 (Ding et al., 2001). Another modification with respect to Anders & Grevesse (1989) comes from a lower sulfur elemental abundance by a factor 0.86, as first deduced by Palme & Beer (1993) and quoted in Lodders (2003) for the solar system. All in all, the solar abundance of ^{36}S is lower than the commonly used Anders & Grevesse (1989) value by a factor 1.6.

The former uncertainty on this isotope extends to its nucleosynthetic origin. The synthesis of the major isotopes of sulfur, similar as for other elements between Si and Fe, can mostly be assigned to charged particle reactions during hydrostatic and explosive burning stages in massive stars: ^{32}S and ^{34}S to hydrostatic and explosive oxygen burning, ^{33}S to explosive oxygen and neon burning (Chin et al. 1996; Woosley et al. 2002). For some exceptionally rare neutron-rich isotopes in this mass range including ^{36}S , however, the situation may be different. ^{36}S has a closed neutron shell, hence a small neutron capture cross section, and in an s-process it could, in principle, act as a bottleneck building up a significant abundance relative to neighboring nuclides. For this reason, the *weak s-process* taking place during core He burning and convective shell C (Ne) burning in massive stars has been suggested as a major source of the ^{36}S abundance in the Solar System (Schatz et al. 1995; Woosley et al. 2002), and according to first network calculations by Schatz et al. (1995) it seemed to be able to fulfill that role. However, re-assessment by Reifarth et al. (2000) with updated nuclear input data indicates a more complex situation. The unexpectedly low neutron capture cross section of ^{34}S causes this nuclide to restrict the flow towards ^{36}S . With rare ^{35}Cl being the main seed nucleus rather than abundant ^{28}Si and ^{32}S , the

weak s-process, while actually making ^{36}S , falls short by more than an order of magnitude in quantity in their assessment. Here, a further complication arises because in all recent calculations the abundance of the major seed, ^{35}Cl , which in the s-process zone is given by its original abundance, has been taken from Table 3 of Anders and Grevesse (1989). Actually, there is disagreement for Cl between the nuclide abundances in their Table 3 and the 39% higher elemental abundance given in their Table 1; the latter agrees with other previous and more recent compilations. The predicted $^{35}\text{Cl}/^{37}\text{Cl}$ ratio is not affected by these changes, but there is a significant effect on the ^{36}S overproduction factor, which is increased by a factor of 1.4.

According to current models, in massive stars most ^{36}S is produced in a large mass zone where convective shell C-burning operates in hydrostatic conditions before the SNII explosion (Woosley & Weaver 1995). Owing to the high neutron density in the first phase of carbon consumption (Raiteri et al. 1992), more ^{36}S is fed through the neutron channel of the unstable ^{35}S than would be inferred by the occurrence of the classical weak s-process. The nucleosynthesis yields of the most recent massive star calculations, made with solar initial composition and with a full network included (Woosley et al. 2002; Rauscher et al. 2002; Limongi & Chieffi 2003), are all based on the Bao et al. (2000) compilation of neutron capture cross sections (where the new and much lower cross section for ^{34}S is included). These results show a production factor of ^{36}S that is typically low by a factor of 2 with respect to the mean of the most abundant nuclides. Taken at face value, this factor of 2 may be reconciled using the new solar ^{36}S abundance as well as the correct ^{35}Cl abundance. However, this does not completely solve the problem of the reproduction of solar ^{36}S , since one would expect the weak s-process products to decline with decreasing metallicity, i.e. earlier generations of massive stars to have been less effective producers of ^{36}S . In addition, there are uncertainties related to the nuclear input data. In particular, the rate of the major channel $^{36}\text{Cl}(n,p)^{36}\text{S}$ may be subject to further refinements in the future owing to the much better energy resolution obtained in the new mea-

surements of Wagemans et al. (2003). On the other hand, recent investigations of n-induced reactions on ^{37}Ar and ^{39}Ar (Goeminne et al. 2000, 2002) seem not to affect the ^{36}S production in a significant manner.

A complementary, though probably less important, source to the weak s-process is the *main s-process* taking place in the He burning shell of low mass AGB stars. According to calculations partially published in Travaglio et al. (2004), the Galactic contribution to ^{36}S at the epoch of Solar System formation by all previous generations of AGB stars is about 4%; this may reach $\sim 10\%$ once the revised lower ^{36}S and higher ^{35}Cl solar abundances are taken into account.

5.4.2. Stellar mass of IRC+10216

In Fig. 5 we show the S isotopic data for IRC+10216 (from this work and Kahane et al. 2000) normalized to ^{34}S and solar system ratios. The data clearly show a more than a factor of 2 enhancement of $^{36}\text{S}/^{34}\text{S}$ in IRC+10216 while the other ratios are solar within error. An s-process enhancement of ^{37}Cl in IRC+10216 was found by Kahane et al. (2000). These authors were able to match the observation with the predictions of a low mass ($1.5 M_{\odot}$) AGB star model of solar metallicity. The enhancement predicted for the envelope after the 15th thermal pulse just corresponded to the observed Cl isotope ratio. Re-analysis, using the updated solar abundances, confirms the agreement, which persists for the last three thermal pulses with dredge-up (#15 to #17). Included in Fig. 5 are the corresponding predictions for the sulfur isotopes (assuming, as in the case of Cl, the updated solar starting composition). It is obvious in Fig. 5 that qualitatively there is agreement between model and observations in that in IRC+10216 an enhancement of only $^{36}\text{S}/^{34}\text{S}$ is seen. However, our observed enhancement of $\sim 170\%$ in this ratio is more than a factor of 4 higher than even the new prediction, which already is about twice as high ($\sim 40\%$ instead of $\sim 20\%$) than that in Kahane et al. (2000).

It has been argued in the past that the central star of IRC+10216 might correspond to an AGB star of intermediate mass, of around $5 M_{\odot}$, instead of the low mass model discussed here. This possibility was at the upper limit of the range of uncertainty of the available distance estimates of 110 — 170 pc (Winters et al. 1994; Crosas & Menten 1997; Le Bertre 1997; Groenewegen et al. 1998; Weigelt et al. 1998). An intermediate mass was inferred by Guélin et al. (1995) on the basis of older estimates of some isotope ratios (see the discussion in Kahane et al. 2000). We have computed a series of AGB models of different initial mass using updated network of neutron capture cross sections and solar abundances. These confirm the conclusions already reached by Kahane et al. (2000) that an intermediate mass of $5 M_{\odot}$ is excluded by the almost solar Mg isotope ratios observed. Indeed, in intermediate mass stars the $^{22}\text{Ne}(\alpha, n)^{25}\text{Mg}$ and $^{22}\text{Ne}(\alpha, \gamma)^{26}\text{Mg}$ reactions would be more efficiently activated by the higher temperature

in the convective He flashes, providing a clear excess of both neutron-rich Mg isotopes. Supporting evidence derives from the observed $^{37}\text{Cl}/^{35}\text{Cl}$ ratio, which would be much higher in an intermediate mass star. The resulting $^{34}\text{S}/^{36}\text{S}$ ratio, in any case, does not depend much on the initial mass.

While the enhancement of the observed $^{36}\text{S}/^{34}\text{S}$ ratio with respect to the $1.5 M_{\odot}$ models could, in principle, be due to some unrecognized problems with the AGB models or assumptions on nuclear parameters involved with it, we believe this to be highly unlikely and the main s-process in IRC+10216 to be not the main source of its (relative to solar) enhanced $^{36}\text{S}/^{34}\text{S}$ ratio. Alternative explanations are briefly discussed below.

5.4.3. Chemical evolution

One clue may be the close agreement between the value for IRC+10216 and the one reported for the ISM (also shown in Fig. 5) by Mauersberger et al. (1996), which at first glance is puzzling. A possible solution may be afforded by Galactic chemical evolution (GCE) and the different times when IRC+10216 and the Solar System formed, i.e. assuming a starting composition different from solar. Based mostly on the $^{12}\text{C}/^{13}\text{C}$ ratio and limits to C/O, Kahane et al. (2000) derived an upper limit of $2 M_{\odot}$ for IRC+10216, which nevertheless still allows the object to be as young as ~ 1.5 Ga. Assuming a correspondingly evolved starting composition, observations might then be compatible (within errors) with model predictions. Indeed, first, there is no need for a large intrinsic contribution to ^{36}S from IRC+10216 (in agreement with the relatively small effect predicted by the AGB star model; Fig. 5). And second, the large difference between the current ISM (and IRC+10216) and the Solar System, is compatible with massive star model predictions, where the ^{36}S Galactic contribution increases with metallicity (as already pointed out by Mauersberger et al., 1996). This would require a rather different evolution of the Cl and S isotopic ratios during the last few Ga, since the observed $^{35}\text{Cl}/^{37}\text{Cl}$ ratio in IRC+10216 is matched by AGB model predictions using solar as the starting composition. Indeed, both Cl isotopes are thought to be synthesized in massive stars in a primary way during explosive Ne and O burning (Weaver & Woosley 1995). Only 4% of the solar abundance of ^{37}Cl is contributed by the main s-component in low mass AGB stars, while ^{35}Cl gets actually depleted by neutron captures, according to the GCE calculations by Travaglio et al. (2004). On the observational side, $^{35}\text{Cl}/^{37}\text{Cl}$ in Orion has been found to be enhanced relative to solar (Salez et al., 1996), but the errors are too large to reach a firm conclusion.

A further possibility is that IRC+10216 simply started with a ^{36}S abundance that was unusually high for its time of formation and location, i.e. invoke inhomogeneity in the ISM. Of course, it could as well be the Solar System rather than IRC+10216 that started out with an unusual com-

position. Both suggestions are not purely ad hoc. Already Lugaro et al. (1999), in order to explain isotopic variations in the Si isotopes of single presolar silicon carbide grains from primitive meteorites, called for small local inhomogeneities in the ISM at the time of parent star formation of the grains as an alternative to Galactic chemical evolution. And, as has been known for quite some time already, oxygen isotopic ratios in the Solar System seem to be quite peculiar (e.g., Wilson & Rood, 1994; Prantzos et al., 1996). In addition, the interstellar Rb isotope ratio $^{85}\text{Rb}/^{87}\text{Rb}$ determined toward ρ Ophiuchi A (Federman et al. 2004) indicates a higher ratio of r- to s-process nuclides in the Solar System as compared to the local ISM.

Reifarth et al. (2000) discussed various other possible nucleosynthesis scenarios besides the s-process. Accepting Galactic chemical evolution as the reason for the difference between the Solar System and the ISM $^{34}\text{S}/^{36}\text{S}$ ratios, those that involve core collapse supernovae (SN) (other than the s-process) face the problem of how to account for the large increase during the last 4.6 Ga. This probably includes the r-process. To some extent this also includes the “neutron burst”, intermediate between s- and r-process and thought to occur during passage of a shock wave through the He shell of type II SN, which Meyer et al. (2000) modelled to explain specific types of isotope abundance anomalies found in supernova grains preserved in meteorites. Note, however, that the efficiency of the process depends on previous s-process seeds and that its effects are included in the SN II yields calculated by the authors cited above. Low-entropy scenarios associated with supernovae type Ia that can account for production of neutron-rich isotopes such as ^{48}Ca and ^{50}Ti (Meyer et al. 1996; Kratz et al. 2001) would be qualitatively compatible with the trend in GCE, but again existing information on production yields for ^{36}S is not encouraging (Reifarth et al. 2000; Kratz et al. 2001).

In summary, while it appears we have observationally identified a stellar source with enhanced ^{36}S and there are some reasonable ideas about how Galactic ^{36}S is produced, we are left with a number of open questions. Further studies of other objects and/or regions in the ISM, especially when correlated with other isotopic systems such as the carbon, oxygen, and chlorine isotopes, may turn out to be helpful. The same holds true for continued study of the relevant stellar physics and nucleosynthesis processes.

6. Conclusions

The main conclusions of this paper are:

1. Measuring the rare isotopic species of CS and SiS in IRC+10216, the abundance ratio of $^{34}\text{S}/^{36}\text{S}$ in IRC+10216 is $107(\pm 15)$, comparable to values in the Galactic interstellar medium (115), but smaller than the solar value (288).
2. The increase of the ^{36}S abundance relative to ^{34}S only qualitatively follows the prediction of a low mass AGB star model. Quantitative agreement of the observed

Table A.1. Line identifications

Nr.	T_A^* mK	Freq. ^a MHz	Im.-Freq. ^a MHz	Identification
1	4	94903	98126	HCCC ^{13}C 36 – 35
2	3.5	94913	98155	SiC $_4$ 32 – 31 (im.)
3	5.5	95018	98011	1-C $_3\text{H}^b$ (im.)
4	6	95035	97095	C ^{36}S ; 1-C $_3\text{H}^b$ (im.)
5	21	95049	97980	CS(2-1) (im.)
6	20	95087	97942	SiC $_4$ 31 – 30
7	1.5	U95115	97914	
8	1.5	95126	97903	SiCCC ^{13}C 32 – 31
9	20	142297	151263	H $_2\text{C}_4$ 16 $_{1,16}$ – 15 $_{2,15}$
10	23	142321	151235	Al ^{37}Cl 10 – 9 ^c
11	3.5	142345	151215	HCCC ^{13}C 54 – 53
12	5	142402	151158	SiS $J = 8 - 7, v = 4^d?$
13	29	142410	151150	NaCN 9 $_{27}$ – 8 $_{26}$
14	5	U142489	151071	
15	40	142502	151058	CCS 11 $_{11}$ – 10 $_{10}^c$
16	7	142525	151035	C ^{36}S 3 – 2 ^c
17	460	142560	151000	^{29}SiS 8 – 7 ^c
18	4	U142594	150966	
19	12	U142622	150940	
20	7	142675	150885	SiCCC ^{13}C 48 – 47
21	9	142695	150865	artefact
22	850	142730	150831	C $_4\text{H}$ $N = 15 - 14^c$
23	9	142755	150805	C $_4\text{H}$ $N = 15 - 14^c$
24	850	142768	150793	C $_4\text{H}$ $N = 15 - 14^c$

a) The band from which the line probably originates is given in bold face; for information, the frequency of the corresponding image band is also given. b) Thaddeus et al. (1985). c) Cernicharo et al. (2000) and references therein. d) The SiS $v = 4 J = 8 - 7$ line is at 142399.8 MHz. A shift of 1 – 2 MHz could be possible if the line is produced in the acceleration region (blue).

$^{34}\text{S}/^{36}\text{S}$ ratio with the stellar models can be reached if the age of IRC+10216 and Galactic Chemical evolution are taken into account or if there are considerable inhomogeneities in the interstellar medium, and either IRC+10216 or the Sun started with an unusual ^{36}S abundance.

3. From the observed line density toward IRC+10216 and toward Galactic star forming regions, confusion limits toward these sources are estimated.

Appendix A: Line identifications

In Table A.1 we list the observed spectral line features seen in Fig. 1, and the approximate values for T_A^* , the rest frequency and the rest frequency in the image band (assuming an LSR velocity of -26 km s^{-1}). The final column contains some identifications from the literature. In the 256 MHz wide spectrum of the C ^{36}S 2 – 1 line we have identified 8 spectral line features. Of those, three can be identified with transitions from the image sideband. In the 256 MHz around the frequency of the C ^{36}S 3 – 2 line we have detected 16 spectral line features, none of which can be assigned to a line from the image band. Six

Table B.1. The confusion limit reached by the IRAM 30-m telescope toward some molecular line sources

Source	λ	weakest detect. Lines	$t_{\text{int}}^{\text{a)}$	Ref. ^b
Δv	mm	mK	h	
IRC+10216 28 km s ⁻¹	3	1.5	28	1)
	2	3.5	10	1, 2)
	1.3	$\lesssim 2$	80	2)
Orion-KL 5 km s ⁻¹	3	20	0.8	3)
	2	50	0.3	4)
	1.3	70	0.4	3)
SgrB2(N) ~ 17 km s ⁻¹	3	~ 20	0.4	3)
	2	~ 30	0.4	3)
	1.3	~ 40	0.5	3)

a) integration time (on+off) with present receivers at the IRAM 30-m telescope under normal winter conditions (good summer conditions), one polarization to obtain an rms of 1/3 T_{mb} with a velocity resolution of 1/5 the line width (one polarization receiver only); b)References: 1) this paper 2) Ziurys et al. (2002); 3) unpublished data; 4) Mauersberger et al. (1988); c) weaker lines can be identified if one makes use of the unique line shapes of the spectra of this source (Cernicharo et al. 2004).

lines can be identified with known transitions from the Cernicharo et al. (2000) line survey, and the other identifications were made with the catalog of the Instituto de la Estructura de la Materia (Madrid) containing ~ 1000 species described by the authors. There is a clearly detected feature at the frequency of the C^{36}S line; another feature at 142.755 GHz is tentatively assigned to emission from C_4S . Eight further lines have not been identified. The emission at 142.695 GHz is an artefact due to some bad spectrometer channels.

Appendix B: The confusion limit toward astronomical molecular line sources

It is evident from Sect. 5.1 that in our 2 and 3 mm spectra of IRC+10216 we are close to the confusion limit, where an increase of integration time does not yield much further information. It is interesting to investigate where line confusion begins to play a role for other favorites of molecule hunters such as the Orion Hot Core, Sgr B2 or the starburst galaxy NGC 253. We limit our discussion to the IRAM-30m telescope. If one wants to extrapolate our results to other telescopes with a higher or lower resolution one has to take into account the detailed source structure chemical and physical conditions within the regions observed (Comito & Schilke 2002).

The definition of the useful observing time or rms to be reached is by no means unique and depends on whether one is interested in a mere detection of a line or whether one also wants to obtain some detailed information on the line shape. Here we try to be pragmatic: we have investigated spectra of several molecular line sources made with the IRAM 30-m telescope at 3 mm, 2 mm and 1.3 mm

wavelength made with such a long integration that $\gtrsim 50\%$ of the spectral range observed is covered with features. We have determined the antenna temperature of the weakest unequivocal line features (knowing the typical line width and shape in the sources studied). The results are given in Table 5.1. We also give an indication of the necessary rms for a 3σ detection with a velocity resolution 1/5 the full line widths typical for these sources and the corresponding necessary integration time with the 30-m telescope and its present receivers (including all observing overheads, using one polarization only). In Orion, part of the confusion arises because of the large line widths observed in the outflow source. This can e.g. be prevented by observing at a carefully selected position offset from the outflow source (Combes et al. 1996).

Acknowledgements. V. Ahrens from the I. Physikalisches Institut der Universität Köln gave us fits to the line frequencies of C^{36}S prior to publication. R.G. acknowledges support by the Italian MIUR-Cofin2002 Project “Nucleosynthesis in the Early Phases of the Universe”.

References

- Anders, E. & Grevesse, N., 1989, *Geochim. Cosmochim. Acta*, 53, 197
- Bao, Z.-Y., Beer, H., Käppeler, F., Voss, F., & Wisshak, K. 2000, *Atomic. Nucl. Data Tables*, 76, 70
- Bevington, P.R., Robinson, D.K., 1992, “Data reduction and error analysis for the physical sciences”, McGraw-Hill
- Biegging, J. H. 1997, *Astrophysical Implications of the Laboratory Study of Presolar Materials*, eds: T. J. Bernatowicz & E. Zimmer, American Institute of Physics, p. 265
- Canfield, D.E. 2001, *Rev. Mineral. Geochem.*, 43, 607
- Cernicharo, J., Guélin, M., & Kahane, C. 2000, *A&AS*, 142, 181
- Cernicharo, J., Pardo, J.R., Guélin, M. 2004, *ApJ Letters*, submitted
- Chin, Y.-N., Henkel, C., Whiteoak, J. B., Langer, N., & Churchwell, E. B. 1996, *A&A*, 305, 960
- Combes, F., Nguyen-Q-Rieu, & Wlodarczak, G. 1996, *A&A*, 308, 618
- Comito, C., & Schilke 2002, *A&A*, 395, 357
- Crosas, M. & Menten, K. M. 1997, *ApJ*, 483, 913
- De Laeter, J. R., Böhlke, J. K., De Bièvre, P., et al. 2003, *Pure Appl. Chem.*, 75, 683
- Ding, T., Valkiers, S., Kipphardt, H., et al. 2001, *Geochim. Cosmochim. Acta*, 54, 2433
- Farquhar, J. & Wing, B.A. 2003, *Earth and Planetary Sci. Letters*, 213, 1
- Federman, S.R., Knauth, D.C., & Lambert, D.L. 2004, *ApJ* 603, L105
- Frum C.I., Engleman Jr., R., Bernath, P.F., 1990, *J. Chem. Phys.*, 93, 5457
- Gao, X. & Thieme, M. H. 1991, *Geochim. et Cosmochim. Acta*, 55, 2671
- Goeminne, G., Wagemans, C., Wagemans, J., et al. 2000, *Nucl. Phys. A*, 678, 11
- Goeminne, G., Wagemans, C., Wagemans, J., et al. 2002, *Nucl. Instr. Meth. Phys. Res. A*, 489, 577
- Grewing, M. 1994, *IRAM Annual Report 1994*, p. 17

- Groenewegen, M. A. T., van der Veen, W. E. C. J., & Matthews, H. E. 1998, *A&A*, 338, 491
- Guélin, M., Lucas, R., & Cernicharo, J. 1993, *A&A*, 280, L19
- Guélin, M., Forestini, M., Valiron, P., Ziurys, L.M., & Anderson, M.A. 1995, *A&A*, 297, 183
- Guélin, M., Cernicharo, J., Travers, M.J., et al. 1997, *A&A*, 317, L1
- Henkel, C. & Mauersberger, R. 1993, *A&A*, 274, 730
- Henkel, C., Wilson, T.L., Langer, N., Chin, Y.-N., & Mauersberger, R. 1994, *The Structure and Content of Molecular Clouds*, Lecture Notes in Physics 439, eds.: T.L. Wilson, K.J. Johnston, Springer Verlag, Heidelberg, p. 72
- Henkel, C., Chin, Y.-N., Mauersberger, R., & Whiteoak, J. B. 1998, *A&A*, 329, 443
- Johansson, L.E.B., Olofsson, H., Hjalmarson, Å, Gredel, R., & Black J.H. 1994, *A&A*, 291, 89
- Kahane, C. 1995, *AIP Conf. Proc.* 327: *Nuclei in the Cosmos III*, 19
- Kahane, C., Gómez-González, J., Cernicharo, J., & Guélin, M. 1988, *A&A*, 190, 167
- Kahane, C., Dufour, E., Busso, M., et al. 2000, *A&A*, 357, 669
- Kratz, K.-L., Böhmer, W., Freiburghaus, et al. 2001, *Mem. S. A. It.*, 72, 453
- Kuiper, T.B.H., Knapp, G.R., Knapp, S.L., & Brown, R.L. 1976, *ApJ*, 204, 408
- Le Bertre, T. 1997, *A&A*, 324, 1059
- Limongi, M. & Chieffi, A. 2003, *ApJ* 592, 404
- Lodders, K. 2003, *ApJ*, 591, 1220
- Lovas, F.J., SLAIM Magnetic tape version T84, priv. comm.
- Lovas, F. J. 1992, *J. Phys. Chem. Ref. Data*, 21, 181
- Lucas, R., Guélin, M., Kahane, C., Audinos, P., & Cernicharo, J. 1995, *Ap&SS*, 224, 293
- Lugaro, M., Zinner, E., Gallino, R., & Amari, S. 1999, *ApJ*, 527, 369
- Mauersberger, R. & Henkel, C. 1989, *A&A*, 223, 79
- Mauersberger, R., Henkel, C., & Wilson, T. L. 1988, *A&A*, 205, 235
- Mauersberger, R., Guélin, M., Martín-Pintado, J., et al. 1989, *A&AS*, 79, 217
- Mauersberger, R., Henkel, C., Langer, N., & Chin, Y.-N. 1996, *A&A*, 313, L1
- Meyer, B.S., Krishnan, T.D., & Clayton, D.D. 1996, *ApJ*, 462, 825
- Meyer, B.S., Clayton, D.D., & The, L.-S. 2000, *ApJ*, 540, L49
- Olofsson, H., Johansson, L.E.B., Hjalmarsson, A., & Nguyen-Q-Rieu 1982, *A&A*, 107, 128
- Palme, H. & Beer, H. 1993, in: *Landolt Börnstein Group VI, Astronomy and Astrophysics, Vol 2A*, ed. H.H. Voigt (Berlin, Springer), p.196
- Prantzos, N., Aubert, O., & Audouze, J. 1996, *A&A*, 309, 760
- Raiteri, C. M., Gallino, R., & Busso, M. 1992, *ApJ*, 387, 263
- Rauch, M. 1998, *ARA&A*, 36, 267
- Rauscher, T., Heger, A., Hoffman, R.D., & Woosley, S.E. 2002, *ApJ*, 576, 323
- Reifarth, R., Schwarz, K., & Käppeler, F. 2000, *ApJ*, 528, 573
- Rosman, K.J.R. & Taylor, P.D.P 1998, *Pure Appl. Chem.*, 70, 217
- Salez, M., Frerking, M. A., & Langer, W.D. 1996, *ApJ*, 467, 708
- Sanz, M.E., McCarthy, M.C., Thaddeus ,P. 2003, *J. Chem. Phys.*, 119, 11715
- Schatz, H., Jaag, S., Linker, G., et al. 1995, *Phys. Rev.*, C51, 379
- Thayer, M. R. 1997, *ApJ* 482, 792
- Thaddeus, P., Gottlieb, C.A., Hjalmarson, Å., et al. 1985, *ApJ*, 294, L49
- Thode, H.G. & Rees, C.E., 1971, *Earth and Planetary Sci. Letters*, 12, 434
- Townes, C.H. & Schawlow, A.L. 1975, *Microwave Spectroscopy*, Dover Publ., New York
- Travaglio, C., Gallino, R., Arnone, E., Cowan, J., Jordan, F., & Sneden, C. 2004, *ApJ*, 601, 864
- Wagemans, C., Goeminne, G., De Smet L., & Wagemans, J. 2003, *Nucl. Phys.*, A719, 127c
- Wall, J.V. & Jenkins, C.R. 2003, "Practical Statistics for Astronomers", Cambridge University Press, Cambridge
- Weigelt, G., Balega, Y., Blöcker, T., et al. 1998, *A&A*, 333, L51
- Wilson, T. L. & Matteucci, F. 1992, *A&A Rev.*, 4, 1
- Wilson, T. L. & Rood, R. 1994, *Ann. Rev. A&A*, 32, 191
- Winters, J.M., Dominik, C., Sedlmayr, E. 1994, *A&A*, 288, 255
- Woosley, S. E. & Weaver, T. A. 1995, *ApJS*, 101, 181
- Woosley, S.E., Heger, A., & Weaver, T.A. 2002, *Rev. Mod. Phys.*, 74, 1015
- Ziurys, L. M., Savage, C., Highberger, J. L., et al. 2002, *ApJ*, 564, L45

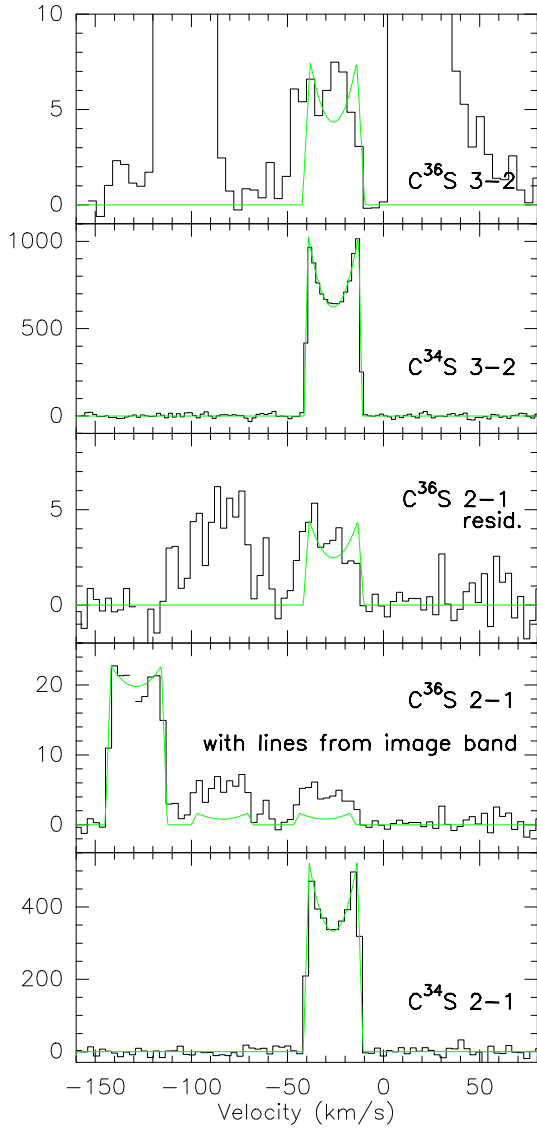


Fig. 2. C^{34}S and C^{36}S $J = 2-1$ and $3-2$ spectra toward IRC+10216. The channel spacing corresponds to 3 km s^{-1} for the $2-1$ lines of C^{34}S and C^{36}S , 2 km s^{-1} for the $3-2$ line of C^{34}S and 4 km s^{-1} for the $3-2$ transition of C^{36}S . Intensities are in mK (T_{A}^*). Also shown are fits (convolved with the channel widths) of a shell type emission profile to the lines. The lineshapes of the C^{36}S transitions were determined from the fits to the corresponding C^{34}S lines. In the frame for C^{36}S ($2-1$), the emission feature at the extreme left corresponds to the $2-1$ line of the main isotope of CS observed in the image band. A fit to the C^{32}S line and to two $\text{l-C}_3\text{H}$ lines from the image band fixing the intensity ratios to the values obtained from a well calibrated spectrum (Mauersberger et al. 1996) is overlaid on the spectrum. In the third frame the residuals obtained from subtracting the fit to the lines from the image sideband are shown.

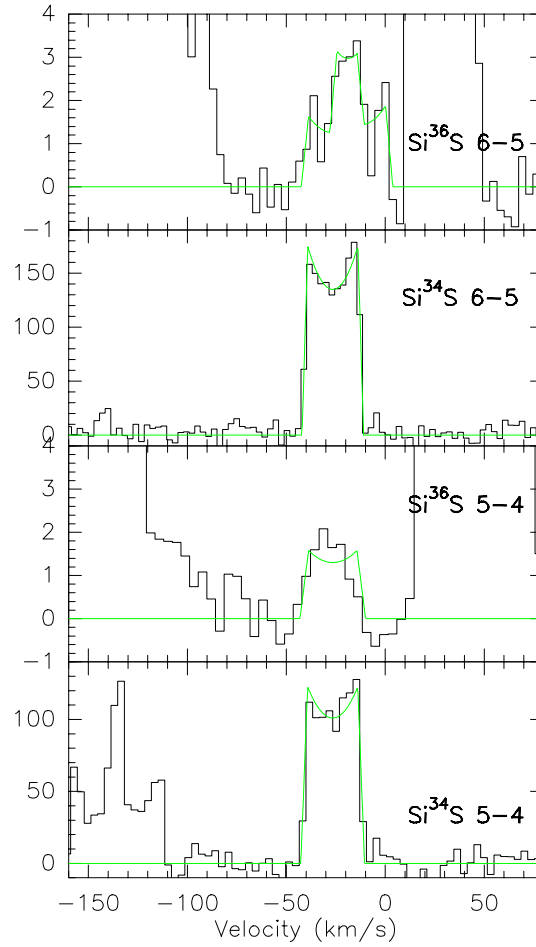


Fig. 3. Si^{34}S and Si^{36}S $J = 5-4$ and $6-5$ spectra toward IRC+10216. The channel spacing corresponds to $\sim 3.5 - 4 \text{ km s}^{-1}$. Intensities are in mK (T_{A}^*). Also shown are fits (convolved with the channel widths) of a shell type emission profile to the lines. In case of the Si^{36}S $J = 6-5$ transition, a simultaneous fit (assuming identical line width) with a blended unidentified line is shown.

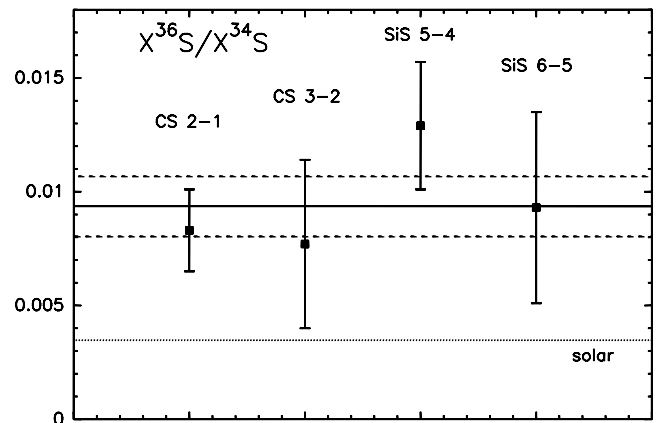


Fig. 4. Isotopic ratios of $^{36}\text{S}/^{34}\text{S}$ obtained from four transitions. The straight line indicates the weighted mean value; a dashed line indicates the error of the mean value. Also shown is the solar system ratio ($3.47 \cdot 10^{-3}$).

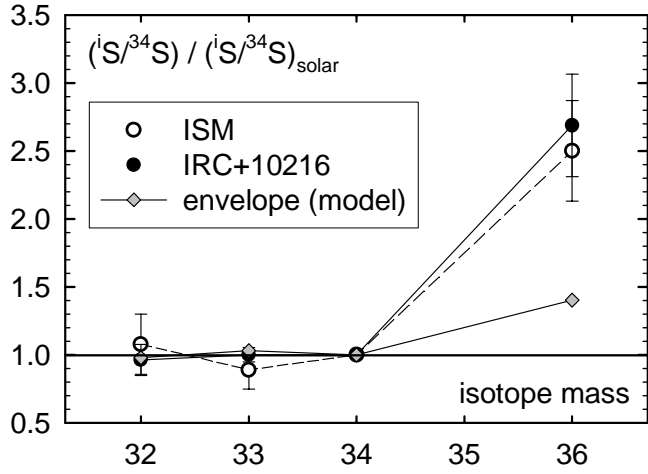


Fig. 5. Sulfur isotopic ratios in IRC+10216, normalized to ^{34}S and solar ratios. Data from Kahane et al. (2000) and this work. Also shown are the S isotope ratios predicted for the envelope of a $1.5 M_{\odot}$ solar-metallicity, TP-AGB star at the time the Cl isotope ratio is matched (see text; with updated solar abundances), and the ratios measured for the ISM by Mauersberger et al. (1996).